DIFFUSION SYNTHETIC ACCELERATION – PART I: DEFICIENCIES IN MULTI–DIMENSIONAL HETEROGENEOUS PROBLEMS

James. S. Warsa, Todd A. Wareing and Jim E. Morel
Transport Methods Group
Los Alamos National Laboratory
Los Alamos, New Mexico 87545

Send proofs to:

James S. Warsa
Los Alamos National Laboratory
CCS–4, MS D409
Los Alamos, NM 87545

E-mail: *warsa@lanl.gov*
FAX: 505-665-5538

Number of pages:	34
Number of figures:	14
Number of tables:	2

DIFFUSION SYNTHETIC ACCELERATION – PART I: DEFICIENCIES IN MULTI–DIMENSIONAL HETEROGENEOUS PROBLEMS

James S. Warsa, Todd A. Wareing and Jim E. Morel
Transport Methods Group
Los Alamos National Laboratory
Los Alamos, New Mexico 87545

Abstract

In this first part of two papers on diffusion synthetic acceleration (DSA) methods, we consider three–dimensional, unstructured tetrahedral meshes using a lumped, linear discontinuous discretization of the first order form of the S_N transport equation. We will identify certain types of multidimensional problems for which established DSA schemes are ineffective and so result in inefficient transport solutions. We consider a fully consistent DSA method in addition to the partially consistent method currently being used in the production transport code AttilaV2. The types of highly diffusive problems for which both DSA methods become ineffective can be generally classified into problems containing highly diffusive regions with large scattering ratios together with large discontinuities in material properties. Effectiveness of the fully consistent method degrades only in the presence of material discontinuities while it is independent of optical thickness. The partially consistent method degrades somewhat scattering ratios are large and cells are optically thick and the presence of material discontinuities makes it worse. We use the results of Fourier analysis and numerical experiments to systematically examine these observations, focusing on the kinds of very diffusive problems for which DSA is most needed.

1 INTRODUCTION

There are many problems of interest for which diffusion synthetic acceleration (DSA) is essential for computing S_N transport solutions in a reasonable amount of time. It is well–known that the discretization of the DSA diffusion equations must be "consistent" with the S_N transport discretization to be effective and robust.[1–3] The effectiveness of DSA can be measured by the spectral radius of the accelerated algorithm. It is always less than one for a useful algorithm and the closer it is to zero, the faster the iteration converges. In the spatially discretized case, consistency is necessary for DSA to achieve the level of acceleration that is predicted analytically.[2,4,5]

In a recent paper, an efficient solution method for the fully consistent, linear discontinuous, finite element (DFEM) diffusion (P_1) equations was developed.[5] Solution of the P_1 linear system was used as a fully consistent DSA (FCDSA) scheme for accelerating the iterative solution of the DFEM discretization of the S_N transport equation on three–dimensional unstructured tetrahedral meshes for isotropically scattering problems. The FCDSA method was compared to two partially consistent methods, the simplified WLA (S–WLA) scheme[6] that is currently employed in the AttilaV2 production code[7] and the Modified Four–Step (M4S) method.[8] An effective DSA scheme is one that results in a large error reduction per iteration. This corresponds to a spectral radius significantly less than one. The effectiveness of a DSA method, however, is not a sure measure of its potential performance. The efficiency of the method also has to be considered. An efficient DSA scheme is one in which the spectral radius small enough *and* the cost of computing the DSA correction is small enough such that the transport solution is computed to a given tolerance with less overall computational effort than would otherwise be possible. In Ref.[5] it was found that the FCDSA method is effective over a wide range of problems but the expense of computing the solution to the consistently discretized P_1 equations is very high and the method is not always efficient. That is, the cost of computing a consistent diffusion correction sometimes overwhelms the reduction in the number of source iterations thus obtained. A partially consistent consistent scheme, such as the Simplified WLA method, was found to be more efficient in some cases, despite being significantly less effective than the fully consistent method.

However, in certain kinds of highly diffusive problems – problems for which DSA is most needed – DSA schemes could lose their effectiveness. A degradation in effectiveness may only occur under certain circumstances, for example, in higher dimensions or on non–rectangular or unstructured meshes. A particular example is the M4S DSA scheme. It was originally shown to be effective for homogeneous problems over a wide range of cell thicknesses both in one dimension and on two–dimensional rectangular grids.[8] In Ref. 5, however, the M4S method was found to be unstable on three–dimensional tetrahedral meshes for cells of intermediate optical thickness. Similarly, the S–WLA method was shown to be unconditionally effective in one dimensional slab geometry[6] but in Ref. 5 it was shown that its effectivness is reduced in problems with optically thick cells and scattering ratios very close to 1.0. Meshes with poorly shaped or skewed cells

(those having both very large and very small interior angles) can make the degradation worse in highly diffusive problems. It was shown in Ref. 5 that the S–WLA effectiveness is further reduced by poorly shaped mesh cells in highly scattering problems and the Modified Four–Step method became unstable for cells with decreasing aspect ratios, but which were still relatively well–formed. FCDSA consistent method was shown to be only slightly affected by cell shape and to a much lesser extent than S–WLA.

Another case in which DSA methods, even fully consistent schemes, can lose their effectiveness is in heterogeneous problems with strong material discontinuities. This is the situation we are concerned with in this paper. Such problems contain two or more materials with total cross sections that vary by as much as several orders of magnitude. The problem may consist of relatively large regions of different materials sharing a common interface or it may be one in which the materials differ from cell–to–cell. Without loss of generality we will limit ourselves to problems with just two different materials. Degradation of the partially consistent S–WLA method occurs on unstructured meshes for problems with optically thick cells and scattering ratios approaching unity regardless of material discontinuities. Introducing material discontinuites only exacerbates the reduction in effectiveness. Degradation of the FCDSA method also occurs in the presence of material discontinuities but if all regions are optically thick, then it remains effective even with large material discontinuities.

The adverse effects of material heterogeneities on DSA methods was noted in Ref. 9 for consistently accelerated even–parity S_N equations in two–dimensional Cartesian geometry. There the degradation of the DSA spectral radius was analyzed and observed numerically using layers of two different materials in a so–called Periodic Horizontal Interface configuration. The authors also point out this effect is not exhibited by consistent methods in one dimension.

Our purpose in this paper – the first of two parts – is to identify certain types of heterogeneous problems that cause a marked decrease in the effectiveness of both the partially consistent S–WLA method and the FCDSA method. We use the same Fourier analysis on three–dimensional tetrahedral meshes as presented in Ref. 5 but modified to account for multiple materials. These analytical predictions are compared to numerical computations for problems in which we see a reduction in DSA effectiveness. We will not consider the M4S scheme because it was found to be unstable. We emphasize that this degradation only appears when the scattering ratios are very close to unity. This may be possible in time–dependent problems of radiative transfer, for example, where the *effective* scattering ratios are very close to one with time steps of typical size.

The rest of the paper is organized as follows. We will present the linear discontinuous discretization and briefly discuss the DSA methods considered in the next section. The following section will present a Fourier analysis of the DSA schemes and establish the classes of problems for which difficulties are expected. In the section after that we will present the results of actual numerical computations with the AttilaV2 host code

that verify the Fourier analysis. The paper concludes with some summary closing remarks.

2 DISCONTINUOUS FINITE ELEMENT DISCRETIZATION ON TETRAHEDRAL MESHES

We will begin by presenting the linear discontinuous finite element method (DFEM) for the transport equation on tetrahedra followed by a brief overview of the fully consistent and partially consistent DSA methods that we consider in this paper. Further details on the fully consistent scheme can be found in Ref. 5 and details of the partially consistent method can be found in Ref. 10.

2.1 Discontinuous Finite Element Discretization

The notation used here has the usual meaning[11] and we assume cgs units. Given an angular quadrature set with N specified nodes and weights $\{\hat{\Omega}_m, w_m\}$, a distributed source of particles $Q(\boldsymbol{r}, \hat{\Omega})$ and anisotropic scattering of order L, the monoenergetic, steady–state S_N transport equation in the three–dimensional domain $\boldsymbol{r} \in V$ with boundary $\boldsymbol{r}_s \in \partial V$, is

$$\hat{\Omega}_m \cdot \nabla \psi_m(\boldsymbol{r}) + \sigma_t(\boldsymbol{r})\psi_m(\boldsymbol{r}) = \sum_{l=0}^{L} \sigma_{s,l} \sum_{n=-l}^{l} Y_{ln}(\hat{\Omega}_m)\phi_l^n(\boldsymbol{r}) + Q(\boldsymbol{r}, \hat{\Omega}_m), \quad m = 1, \ldots, N. \tag{1a}$$

Here, $Y_{ln}(\hat{\Omega})$ are the spherical harmonics functions and the scalar flux moments are

$$\phi_l^n(\boldsymbol{r}) = \sum_{m=1}^{N} w_m Y_{ln}(\hat{\Omega}_m)\psi_m(\boldsymbol{r}). \tag{1b}$$

We assume that the quadrature, cross sections, and spherical harmonics are appropriately normalized. Boundary conditions are specified on the surface $\boldsymbol{r}_s$ with outward unit normal $\hat{n}$ by

$$\psi_m(\boldsymbol{r}_s) = \Gamma(\hat{\Omega}_m) \quad \text{for} \quad (\hat{n} \cdot \hat{\Omega}_m) < 0. \tag{1c}$$

For the remainder of both parts of this paper we will assume only isotropic scattering, for which we set $L = 0$ and $\sigma_{s,0} = \sigma_s$. The inhomogeneous source is also assumed to be isotropic, or $Q(\boldsymbol{r}, \hat{\Omega}) = Q_0(\boldsymbol{r})$. We will consider vacuum boundary conditions, $\Gamma(\hat{\Omega}_m) = 0$, isotropic incident boundary sources, $\Gamma(\hat{\Omega}_m) = \Psi_0$, or specular reflection boundary conditions, in which case $\Gamma(\hat{\Omega}_m) = \psi_{m'}(\boldsymbol{r}_s)$. In the latter case, the reflected image of $\hat{\Omega}_m$, denoted by $\hat{\Omega}_{m'}$, is defined by

$$\hat{\Omega}_{m'} = \hat{\Omega}_m - 2\,\hat{n}\left(\hat{\Omega}_m \cdot \hat{n}\right). \tag{1d}$$

Therefore, we set $\Gamma(\hat{\Omega}_m) = \psi_{m'}(\boldsymbol{r}_s)$ on reflective boundaries, where Eq. 1d determines m'.

The linear DFEM discretization is specified by the following variational formulation. It is written in source iteration form with iteration index ℓ. Given an angular flux expansion in terms of the four independent linear basis functions on a tetrahedral cell T_k,

$$\psi_{m,k} = \sum_{j=1}^{4} \psi_{m,j,k} L_j(\boldsymbol{r}), \tag{2}$$

find the linear approximation for each angle $\hat{\Omega}_m$ that satisfies

$$\hat{\Omega}_m \cdot \left(\int_{\partial T_k} \hat{n}\, \psi_m^b\, u_k\, dS - \int_{T_k} \psi_{m,k}^{\ell+1} \nabla u_k\, dV \right) + \sigma_{tk} \int_{T_k} \psi_{m,k}^{\ell+1}\, u_k\, dV = \sigma_{sk} \sum_m w_m \int_{T_k} \psi_{m,k}^{\ell}\, u_k\, dV + \int_{T_k} Q_m u_k\, dV \tag{3a}$$

for all trial functions u_j on cell T_k. The Galerkin approximation takes the trial functions to be the basis functions themselves and the above expressions can be evaluated for each of the four trial functions. This gives four equations for the four unknowns $\psi_{m,j,k}$ on the cell. Before carrying out the integrations in Eq. 3a, however, we first introduce the discontinuous approximation. Considering a cell k with face j whose outward normal is $\hat{n}_j$, the boundary terms $\psi_{m,j}^b$ are defined as

$$\left(\hat{\Omega}_m \cdot \hat{n}_j\right) \psi_{g,m}^b = \begin{cases} \left(\hat{\Omega}_m \cdot \hat{n}_j\right) \psi_{g,m,i(j),s}, & \hat{\Omega}_m \cdot \hat{n}_j > 0, \quad \hat{n}_j \text{ in } V \\ \left(\hat{\Omega}_m \cdot \hat{n}_j\right) \psi_{g,m,i(j),l}, & \hat{\Omega}_m \cdot \hat{n}_j < 0, \quad \hat{n}_j \text{ in } V \backslash \partial V \\ \left(\hat{\Omega}_m \cdot \hat{n}_j\right) \Gamma(\hat{\Omega}_m), & \hat{\Omega}_m \cdot \hat{n}_j < 0, \quad \hat{n}_j \text{ on } \partial V \end{cases} \tag{3b}$$

where l is the cell that shares face j with cell s. The subscript $i(j)$ denotes three vertices i on a face j of a given cell. Simply put, if $\boldsymbol{n}_j$ is on the boundary of the problem domain V, then the boundary condition is used to define the incoming angular flux; otherwise the internal or external values angular fluxes are used depending on the orientation of the cell face with respect to the quadrature direction. The discrete boundary conditions are vacuum, $\Gamma(\hat{\Omega}_m) = 0$, or $\Gamma(\hat{\Omega}_m) = \psi_{g,m',i(j),s}$ for reflective boundary conditions, where m' satisfies Eq. 1d for $\hat{\Omega}_m$ and $\hat{n} = \hat{n}_j$. Reflection is implemented only for boundary faces aligned parallel to the x, y or z coordinate axes such that the standard quadrature sets we use contain the reflected angles that satisfy Eq. 1d.

Having evaluated Eq. 3 (either analytically or by quadrature approximation) for every cell in the mesh, the angular flux, $\psi_{m,i,j}$, can be computed for all vertices $j = 1, 4$ of every cell k, one cell at a time over the entire mesh. This is done in a predetermined order for every quadrature angle $\hat{\Omega}_m$. The process, called an angular sweep, is repeated at every source iteration.

Note that Eq. 3a can be written in operator notation as

$$\boldsymbol{L}_m \psi_m^{\ell+1} = \boldsymbol{S}\phi^{\ell} + Q, \quad \phi^{\ell} = \boldsymbol{K}\psi_m^{\ell}, \quad \boldsymbol{B}\psi_m = g_m, \tag{4}$$

given some initial guess ϕ^0 to the the scalar flux. Boundary conditions are represented by the angular function g_m.

Details of the discretization can be seen in Appendix A, which includes a description of the asymptotic–preserving lumping on tetrahedra used in AttilaV2. This lumped, linear discontinuous scheme not only preserves the diffusion limit but is found to be robust over a wide range of problems.

2.2 DSA Methods

It is easy to see that the convergence of source iteration, which is also known as Richardson or simple iteration, is governed by the spectral radius of the operator $(\boldsymbol{L}_m^{-1}\boldsymbol{S})$. The spectral radius is bounded above by the maximum scattering ratio $c = \sigma_{sk}/\sigma_{tk}$ on the mesh (we assume $c \leq 1$).[2] This implies that for highly scattering, diffusive problems with $c \approx 1$ this iteration is expected to converge slowly, making a solution costly or even impractical. Diffusion synthetic acceleration modifies the source iteration algorithm by computing a correction to the scalar flux, where the diffusion equation is used as an approximation to the transport operator.[2,12–14] For homogeneous problems it can be shown that DSA reduces the spectral radius to approximately $0.225c$, without angular discretization.[2,5]

Although the details are very well–known, we will briefly review the DSA method now to put it in context. We will ignore boundary conditions for purposes of discussion. What is stated here holds for source or boundary conditions with only slight changes needed for reflective boundary conditions. Operating on Eq. 4 with $\boldsymbol{K}$ the iteration for the scalar flux can be written as

$$\phi^{\ell+1} = \boldsymbol{T}\boldsymbol{S}\phi^{\ell} + b \tag{5}$$

where $\boldsymbol{T} = \boldsymbol{K}\boldsymbol{L}_m^{-1}$ and $b = \boldsymbol{T}Q_0$. This is a Richardson iteration for the operator $\boldsymbol{A} = (\boldsymbol{I} - \boldsymbol{T}\boldsymbol{S})$. If ϕ is the exact solution to Eq. 5 then the error $f^{\ell+1} = (\phi - \phi^{\ell+1})$ satisfies

$$(\boldsymbol{I} - \boldsymbol{T}\boldsymbol{S})f^{\ell+1} = \boldsymbol{T}\boldsymbol{S}r^{\ell}, \tag{6}$$

where $r^{\ell} = (\phi^{\ell+1} - \phi^{\ell})$ is the residual. Equation 6 suggests that we can use an approximation to the operator $(\boldsymbol{I} - \boldsymbol{T}\boldsymbol{S})^{-1}\boldsymbol{T}\boldsymbol{S}$ to estimate the error and correct the current iterate. This will lead to a more efficient iteration if the approximate operator is relatively easy to setup and invert and if the approximate operator adequately reduces the spectral radius.

In the case of DSA, the approximate operator involves the diffusion operator, $\boldsymbol{D}$. This is an appropriate choice because the diffusion equation is the asymptotic limit of the transport operator in highly diffusive regimes.[15,16] This is just the situation for which we need acceleration. The diffusion operator is effective because it accounts for those errors which are poorly attenuated by source iteration. Whether the diffusion

operator can be inverted easily and result in a more efficient algorithm depends on the spatial discretization of both the transport equation and the diffusion equation. Introducing an intermediate correction step in the source iteration algorithm, the DSA algorithm is

$$\phi^{\ell+1/2} = \boldsymbol{T}\phi^{\ell} + b \tag{7a}$$

$$f^{\ell+1/2} = \boldsymbol{D}^{-1}\boldsymbol{S}\left(\phi^{\ell+1/2} - \phi^{\ell}\right) \tag{7b}$$

$$\phi^{\ell+1} = \phi^{\ell+1/2} + f^{\ell+1/2}. \tag{7c}$$

The operator $\boldsymbol{D}^{-1}$ represents the "action" of the diffusion operator on the quantity $\boldsymbol{S}\left(\phi^{\ell+1/2} - \phi^{\ell}\right)$. Analytically the operator $\boldsymbol{D}$ is the diffusion equation and $\boldsymbol{D}^{-1}$ is simply its inverse. In the discrete case, however, $\boldsymbol{D}^{-1}$ not only represents the inverse of spatially discretized diffusion equation because certain there may be certain projection and interpolation operations that are needed as well. It is the properties of all the computations represented by the $\boldsymbol{D}^{-1}$ operator that determines how effective, efficient and robust the overall DSA algorithm will be in practice. Foremost among these properties is the spatial discretization of the diffusion equation; it must be consistent in a certain sense with the discretization of the transport operator for DSA to be effective.[2,14] It is possible, however, that consistent discretizations could be difficult to derive or impractical to implement and solve. Furthermore, we will see in this paper that consistency alone does not guarantee an unconditionally efficient algorithm.

For our purposes here, we will consider two different definitions for the operator $\boldsymbol{D}^{-1}$. One is the fully consistent method based on a discontinuous discretization of the P_1 equations that has been described in Ref. 5. Solution of the corresponding large, sparse, linear system gives the necessary discontinuous scalar flux corrections directly. Unfortunately, we found this linear system (which can be written either in symmetric, indefinite form or nonsymmetric, positive definite form) was very difficult to solve. Despite the very effective preconditioner we developed for the iterative solution of these equations, the overall DSA accelerated transport solution cost did not improve in all cases. The other DSA method we will look at is a partially consistent scheme, the S–WLA method. The basic theme of the method is quite simple. A finite element projection of the residual in the discontinuous scalar fluxes is computed. This is used as the source term for a linear continuous finite element diffusion equation for the scalar fluxes centered on the mesh vertices. The linear system is symmetric and positive definite so it can be solved efficiently with conjugate gradient iterations. From the resulting solution on the vertices, a correction to the discontinuous scalar fluxes is computed using the approach described in Ref. 10 for general meshes and arbitrary geometry combined with the lumping described in Appendix A. For reflective conditions, the linear continuous diffusion equation source includes a projection of the residual in the scalar fluxes composed from the angular fluxes on the reflective boundary faces. These angular fluxes are then corrected based on the diffusion equation

solution.

Both of these methods will be examined in the following sections through Fourier analysis and numerical examples. A fully consistent scheme should be the best possible method while a partially consistent or inconsistent method is expected to be somewhat less efficient. We will find, however, that neither method is unconditionally effective in the kinds of problems we consider here.

3 FOURIER ANALYSIS

In this section we present a three–dimensional Fourier analysis on tetrahedra that we apply to the source iteration convergence of both the FCDSA and S–WLA methods. The classes of problems for which the fully and partially consistent methods lose their effectiveness are identified.

The Fourier analysis begins by dividing a three–dimensional box, or basic element, into six tetrahedra of equal volume. The orientation of the tetrahedra cell edges with this subdivision allows us to "tile" a volume with these basic elements. The box is of dimension $(\Delta x \times \Delta y \times \Delta z)$ as shown in Fig. 1. We can analyze the effects of material discontinuities for heterogeneous problems by assigning total cross sections $\sigma_{t,1}$ and $\sigma_{t,2}$ to the two halves of the basic element as indicated, each half consisting of three tetrahedra. The

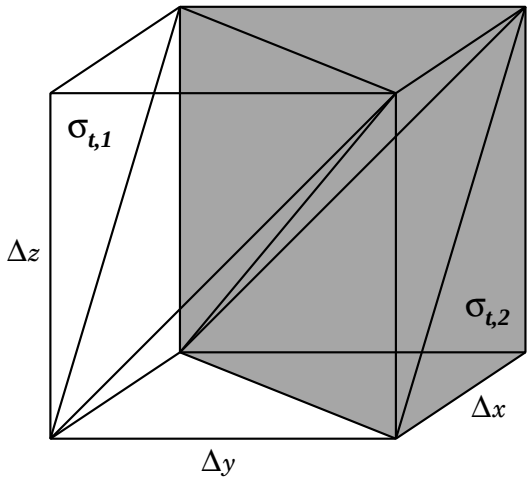

Figure 1: The basic element divided into 6 tetrahedra of equal volume. The two regions, each of which consists of three tetrahedra, contain materials with total cross sections $\sigma_{t,1}$ and $\sigma_{t,2}$.

Fourier analysis procedure is implemented via the symbolic algebra program MAPLE, the details of which are described in Ref. 5. The procedures outlined there have been modified to account for two materials. This basic element is assumed to repeat periodically in three dimensions through a Fourier ansatz of both the discontinuous and the continuous, vertex–centered unknowns. The transport and DSA equations are written by MAPLe in terms of the Fourier ansatz and the 24×24 matrices are translated to Fortran. They can then be evaluated as a function of the element dimensions Δx, Δy, and Δz, the material properties c, $\sigma_{t,1}$ and $\sigma_{t,2}$, and the Fourier wave vector $[\lambda_x, \lambda_y, \lambda_z] \in [0, 2\pi] \times [0, 2\pi] \times [0, 2\pi]$. The space of wave numbers

is searched with a simplex optimization algorithm to find the maximum eigenvalue for a set of dimensions and material properties, which gives a prediction of the spectral radius and, hence, the convergence rate of the transport source iteration.

The spectral radius predicted by Fourier analysis was calculated over a range of cross sections, scattering ratios, and cell shapes in an attempt to account for the range of problems we expect to encounter in our applications. An S_4 triangular Chebyshev–Legendre quadrature is used for which the analytical DSA spectral radius is $0.2543c$. The dimensions of the box are fixed $\Delta x = \Delta z$ $1.0cm = \Delta y = 1.0cm$ and the total cross sections in the two regions are varied over six orders of magnitude. For the scattering ratios $c = 0.9999, 0.999, 0.99$, and 0.9, the results for the S–WLA method are shown in Figs. 2 –5 and results for the FCDSA method are shown in in Figs. 6 – 9. Each plot has eleven curves on it that show the variation in the spectral radius as $\sigma_{t,2}$ is varied for fixed values of $\sigma_{t,1}$. Note that the curves for $\sigma_{t,1} < 1$ have their minimum near the analytical value. Clearly there is a strong dependence on the scattering ratio in the problem as c approaches 1.0 which is more pronounced for the partially consistent DSA scheme in the optically thick limit. When the one of the cross sections is very large, FCDSA is much more effective than the S–WLA method and it does even better when both cross sections are large, independent of the scattering ratio. Aside from the differences in this thick limit between the two DSA methods, the most important observation to note is that neither method can be reliably depended upon to reduce the spectral in heterogeneous problems as $c \longrightarrow 1$. It is now clear that consistency alone does not ensure that a DSA method will be unconditionally effective in all problems.

We end this section by noting that it may be possible to restore, to some extent, the effectiveness of the DSA methods in the strongly heterogeneous problems by setting the total cross section in the optically thin regions to some fixed value. For the FCDSA method, this could be done in both the first moment and balance equations, or just the first moment equation alone. Similarly, for the S–WLA method, this could be done in the diffusion coefficient and the absorption cross section, or in the diffusion coefficient alone. However, it is difficult to determine an appropriate value for this parameter. We have found that it depends very strongly on the problem and that there is an optimal value which may in general be difficult to determine a priori. This is not very satisfactory so we will not pursue at this time.

4 NUMERICAL RESULTS

In this section we present the results of numerical computations with the unstructured tetrahedral mesh transport code AttilaV2. These computations are carried out for the kinds of difficult problems identified by the Fourier analysis in the previous section. They are intended to verify the results of the Fourier analysis and confirm the degraded effectiveness of the DSA schemes in a realistic problem. Throughout, total cross sections have units of cm^{-1}.

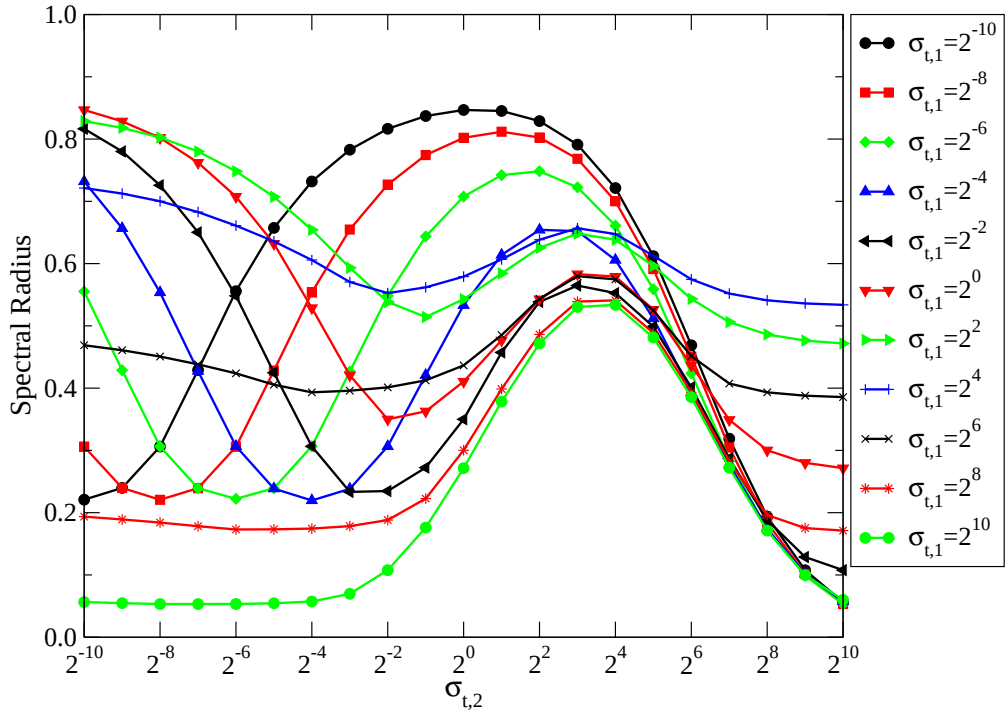

Figure 2: Fourier analysis for the S–WLA method in heterogeneous problems with $c = 0.9$ and total cross sections $\sigma_{t,1}$ and $\sigma_{t,2}$.

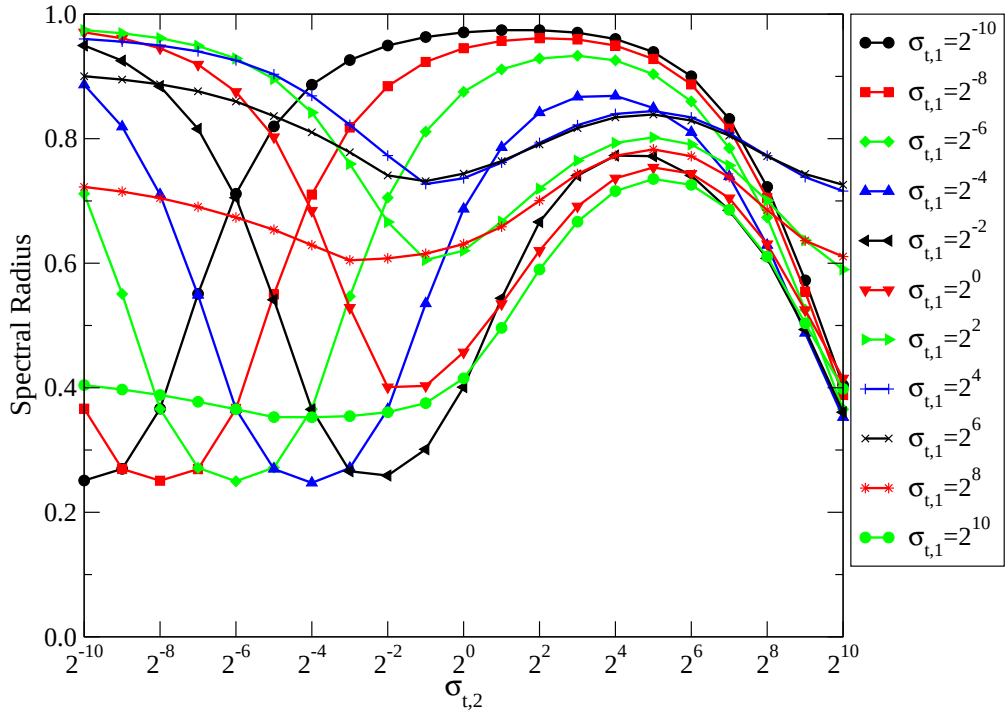

Figure 3: Fourier analysis for the S–WLA method in heterogeneous problems with $c = 0.99$ and total cross sections $\sigma_{t,1}$ and $\sigma_{t,2}$.

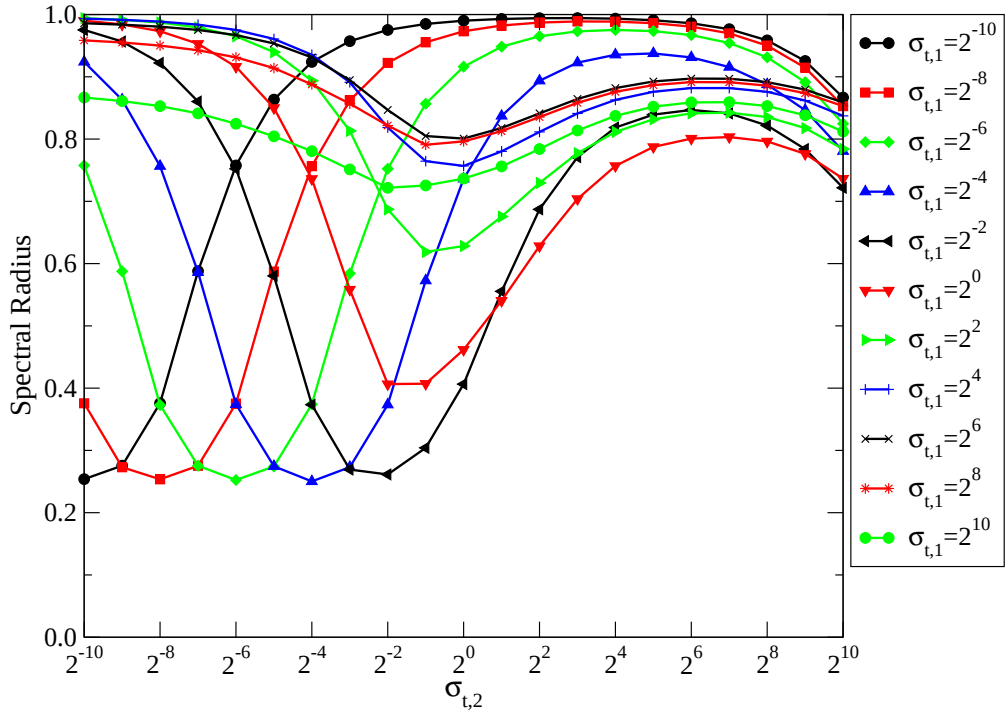

Figure 4: Fourier analysis for the S–WLA method in heterogeneous problems with $c = 0.999$ and total cross sections $\sigma_{t,1}$ and $\sigma_{t,2}$.

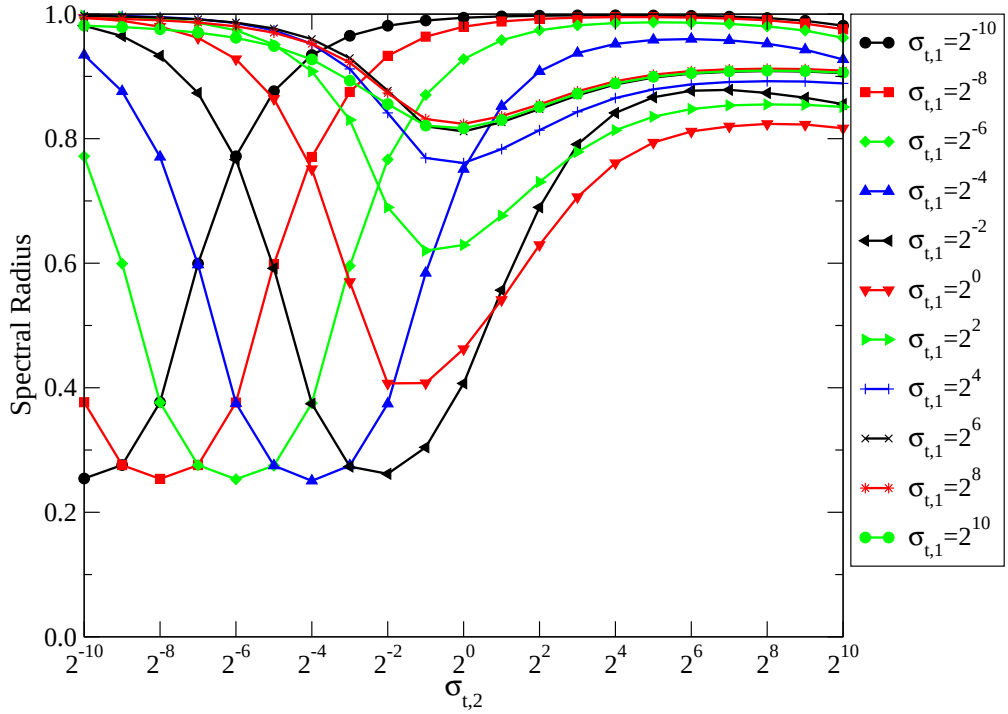

Figure 5: Fourier analysis for the S–WLA method in heterogeneous problems with $c = 0.9999$ and total cross sections $\sigma_{t,1}$ and $\sigma_{t,2}$.

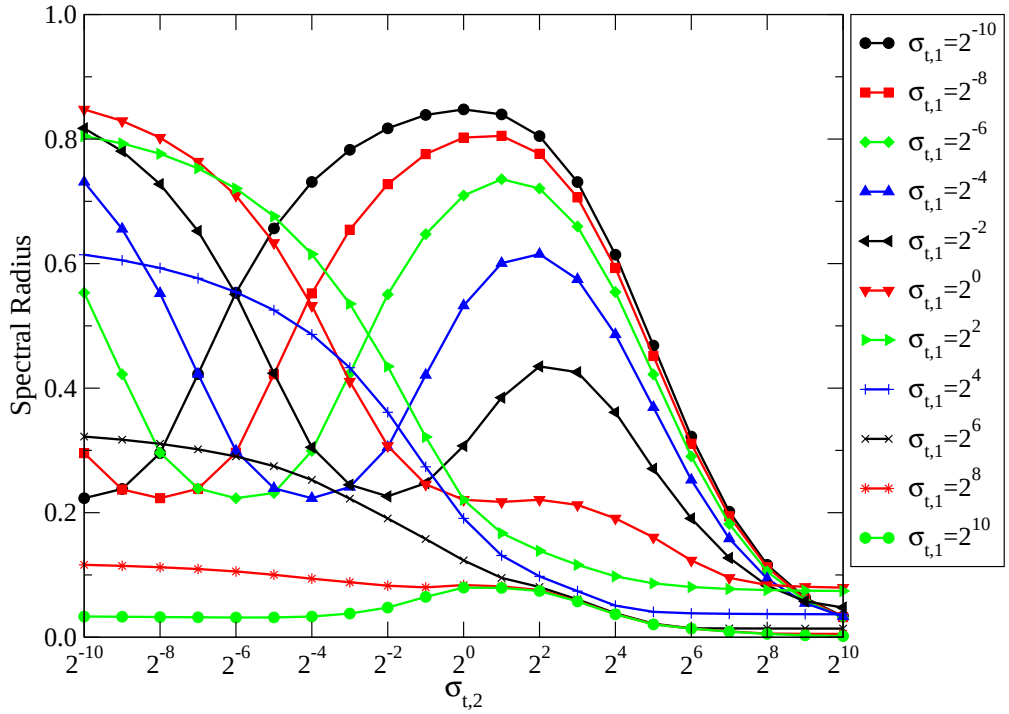

Figure 6: Fourier analysis for the FCDSA method in heterogeneous problems with $c = 0.9$ and total cross sections $\sigma_{t,1}$ and $\sigma_{t,2}$.

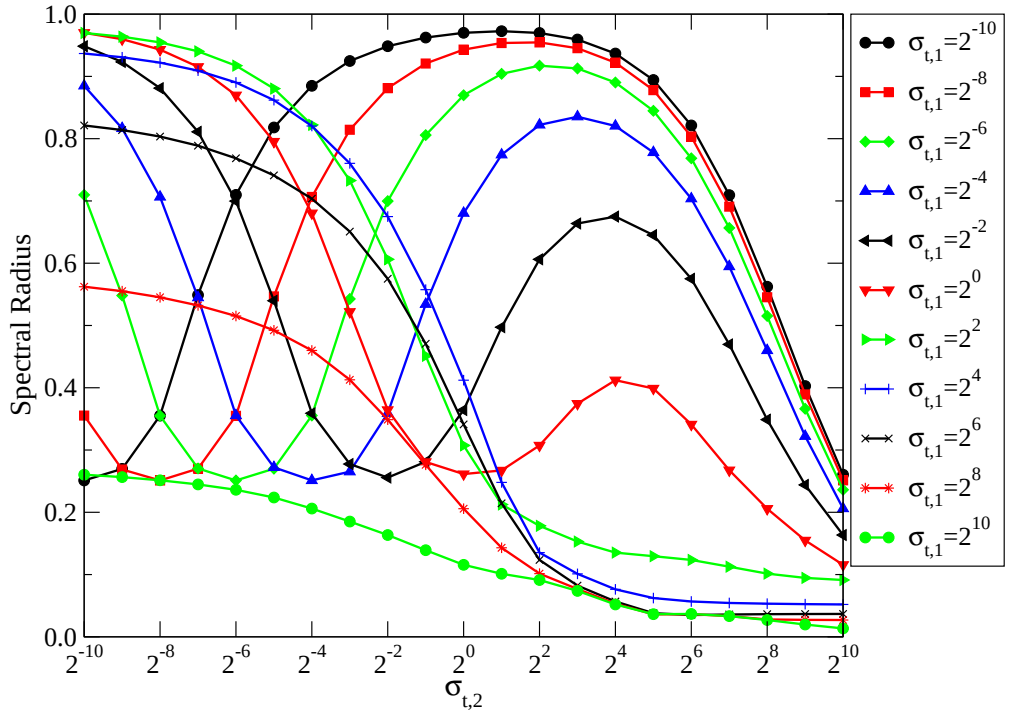

Figure 7: Fourier analysis for the FCDSA method in heterogeneous problems with $c = 0.99$ and total cross sections $\sigma_{t,1}$ and $\sigma_{t,2}$.

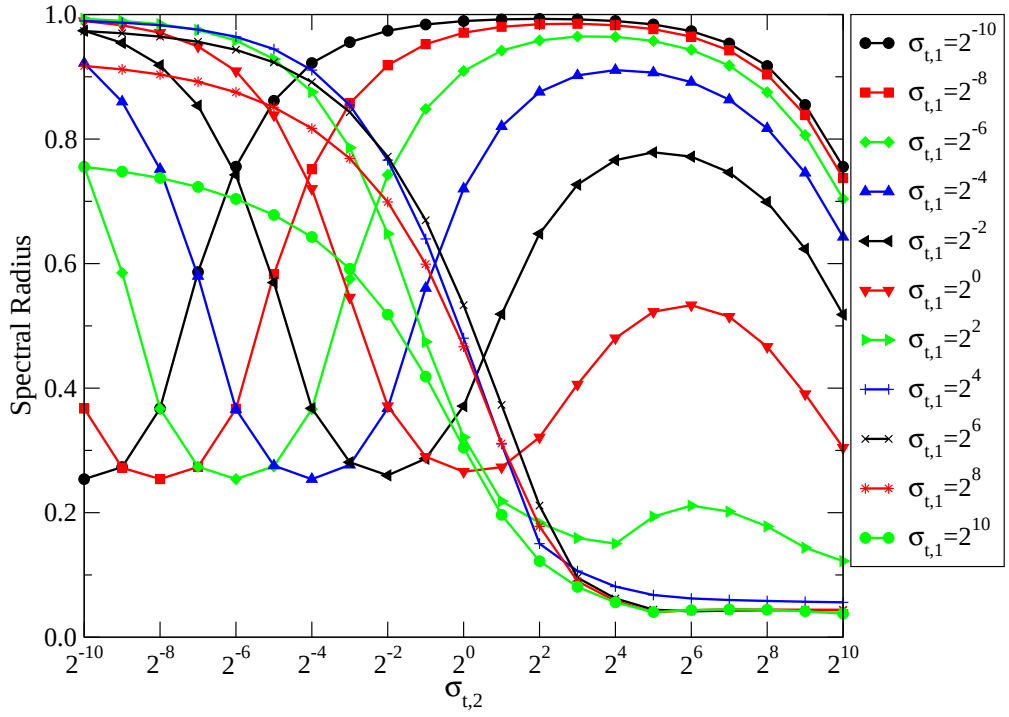

Figure 8: Fourier analysis for the FCDSA method in heterogeneous problems with $c = 0.999$ and total cross sections $\sigma_{t,1}$ and $\sigma_{t,2}$.

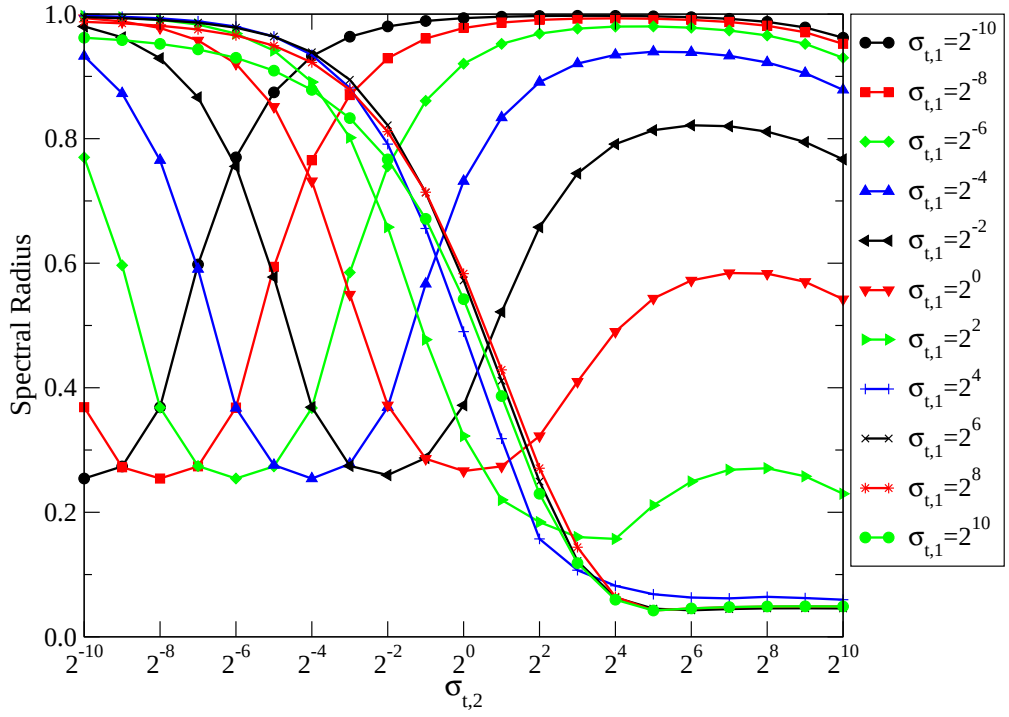

Figure 9: Fourier analysis for the FCDSA method in heterogeneous problems with $c = 0.9999$ and total cross sections $\sigma_{t,1}$ and $\sigma_{t,2}$.

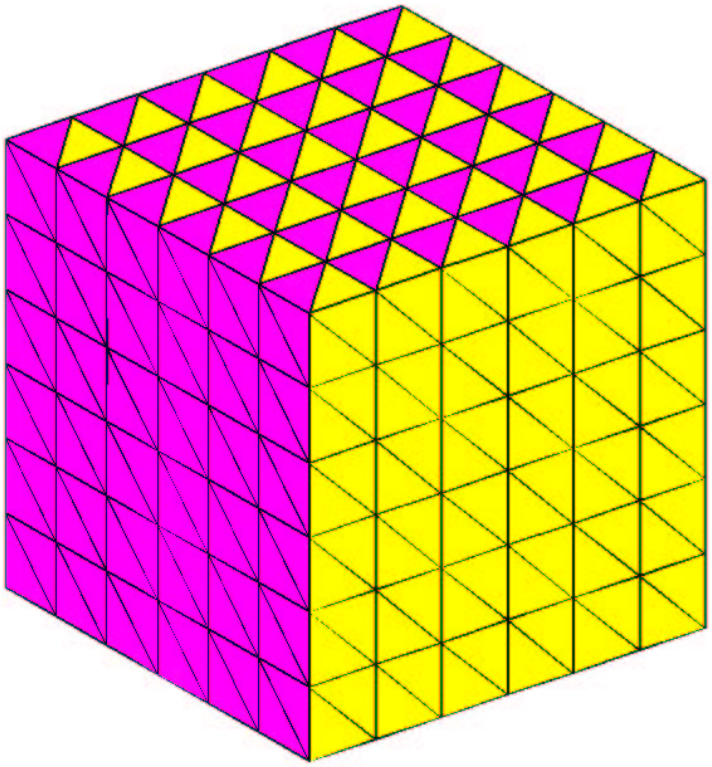

Figure 10: Two material mesh used to compare the Fourier analysis spectral radius predictions with actual computations with AttilaV2. This is $(6 \times 6 \times 6)$ grid of cubes, 1.0 cm on a side, each divided into two sets of three tetrahedra with a different material in each set, as indicated by the shading in the figure.

The first set of results is for a mesh consisting of a $(6 \times 6 \times 6)$ "grid" of cubes, each (1.0 cm on a side. Every cube is divided into six tetrahedra, three of which have total cross section $\sigma_{t,1}$ and three of which have total cross section $\sigma_{t,2}$. This is just like the basic element used for the Fourier analysis in the previous section. An illustration of the mesh is shown in Fig. 10. The boundary conditions are vacuum on the six faces of the problem and the scattering ratio is fixed at $c = 0.999$.

We compare the results of the previous section to the spectral radius measured with AttilaV2 for this problem. Starting with a random initial guess, the spectral radius is estimated by taking the ratio of the residual at two successive iterations, that is,

$$\rho \approx \frac{\|\phi^{\ell+1} - \phi^{\ell}\|_2}{\|\phi^{\ell} - \phi^{\ell-1}\|_2},$$

and renormalizing the scalar flux to $\|\phi^{l+1}\|_2$ after each iteration ℓ. The value reported after 100 iterations is shown in the figures, which we observed were more than enough to reach a value that was not changing in the fourth digit. The stopping tolerance used in the inner DSA iterations was fixed at 10^{-6}. Fig. 11 shows the spectral radius measurements for the S–WLA method for fixed $\sigma_{t,1} = 2^{-2}, 2^{4}, 2^{10}$ as $\sigma_{t,2}$ is varied compared to the Fourier analysis of the previous section. Fig. 12 shows the same set of measurements made

using the FCDSA method. The measured values agree very well with the Fourier analysis. However, when the cross sections are small and the problem domain is optically thin, leakage from the problem reduces the spectral radius relative to the Fourier analysis, which implicitly assumes an infinite, periodic medium. These results confirm that the degradation in heterogeneous problems predicted by the Fourier analysis occurs in actual computations.

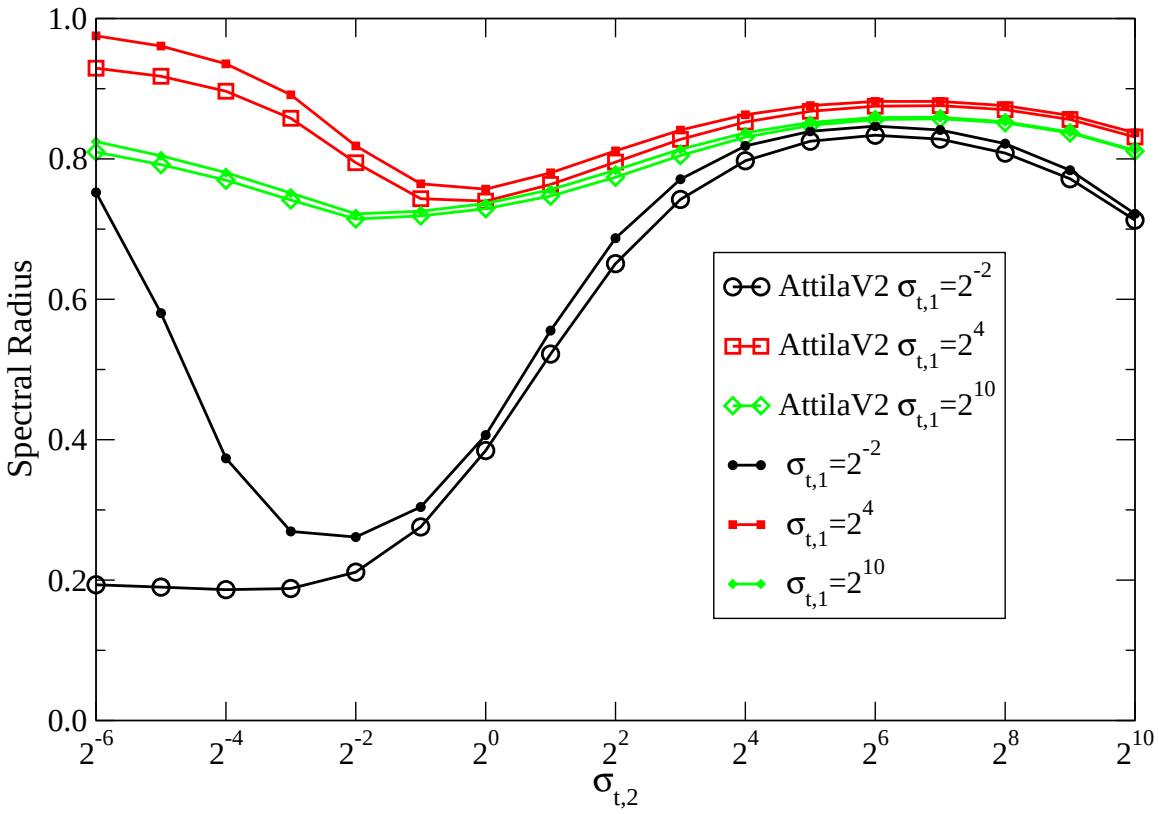

Figure 11: The spectral radius for the S–WLA method with $c = 0.999$ measured with the AttilaV2 code and compared to selected Fourier analysis results from the previous section.

The next set of results are for solutions to a more realistic problem. The mesh consists of two regions, a box with total cross section $\sigma_{t,1}$, centered inside of a hemisphere with total cross section $\sigma_{t,2}$. The half–sphere has a 10 cm radius and the box is $10\sqrt{2}$ cm on a side and 5 cm tall. The mesh is illustrated in Fig. 13. The bottom of the entire hemisphere has a reflective boundary condition, the remainder being vacuum. An isotropic unit source is distributed throughout the box. The scattering ratio is $c = 0.9999$.

Using AttilaV2 on a serial SGI Origin 2000 processor, we measured the number of iterations and number of floating point operations (FLOP) for convergence to a relative residual of 10^{-6} for this problem. A fixed stopping criteria of 10^{-7} was used for the inner DSA iterations. The measurements are shown in Tables 1 and 2. The results are revealing. Firstly, note the two ranges of degradation in the upper right

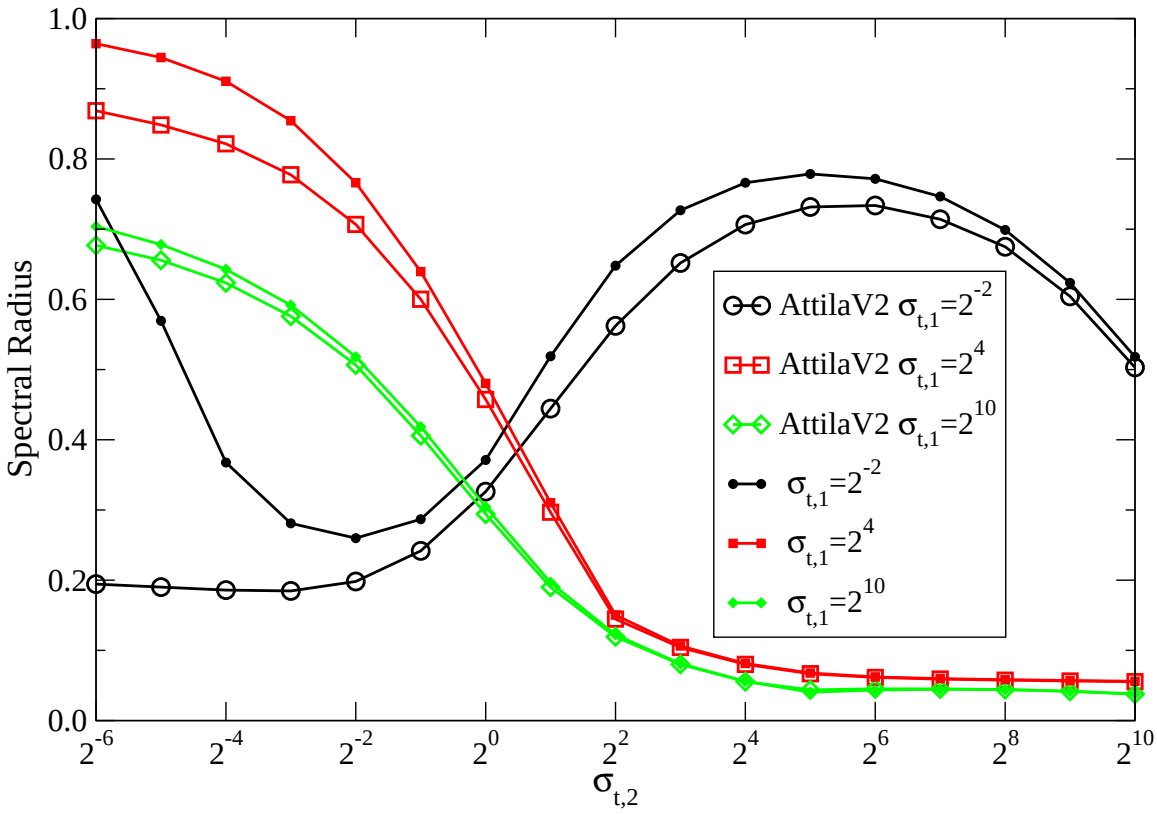

Figure 12: The spectral radius for FCDSA mwith $c = 0.999$ measured with the AttilaV2 code and compared to selected Fourier analysis results from the previous section.

and lower left parts of both tables. These correspond to regions containing optically thin and thick regions in the same problem, confirming that DSA does indeed degrade in this kind of situation, even in realistic calculations. The iteration counts indicate the same kind of dependence on the two total cross sections as seen in the Fourier analysis of the previous section. Secondly, note that even when both regions are optically thick, S–WLA is not very effective while the FCDSA method is extremely effective in this range of optical thickness. Finally, despite the fact that FCDSA reduces the spectral radius and hence the number of iterations, the FLOP counts clearly indicate the high costs associated with solving the fully consistent DSA equations. This renders the method impractical as a general purpose method for transport acceleration.

5 SUMMARY

We have seen that for certain problems of interest, in particular those containing highly diffusive, thick mesh cells in combination with optically thin mesh cells, both fully consistent (FCDSA) and partially consistent (S–WLA) methods can lose their effectiveness. This is an undesirable situation for the following reasons. The linear systems involved in the fully consistent method are very large and difficult to solve. This means

$\sigma_{t,1}$	$\sigma_{t,2}$										
	2^{-10}	2^{-8}	2^{-6}	2^{-4}	2^{-2}	2^{0}	2^{2}	2^{4}	2^{6}	2^{8}	2^{10}
2^{-10}	4	4	6	8	11	16	nc	nc	nc	nc	nc
2^{-8}	5	5	6	8	11	16	22	26	29	28	22
2^{-6}	6	6	6	8	11	16	21	25	28	27	21
2^{-4}	9	9	9	9	10	14	18	22	24	24	19
2^{-2}	13	13	13	12	10	10	13	15	17	17	14
2^{0}	17	17	16	15	11	8	7	9	10	10	9
2^{2}	17	17	17	15	12	8	5	5	6	6	6
2^{4}	15	15	15	14	12	8	5	4	4	4	4
2^{6}	14	14	14	14	12	8	5	4	4	4	4
2^{8}	15	14	14	14	12	9	6	4	4	4	4
2^{10}	14	14	14	14	12	9	6	4	4	4	4

(a) Number of iterations

$\sigma_{t,1}$	$\sigma_{t,2}$										
	2^{-10}	2^{-8}	2^{-6}	2^{-4}	2^{-2}	2^{0}	2^{2}	2^{4}	2^{6}	2^{8}	2^{10}
2^{-10}	49.9	61.2	139	149	170	222	nc	nc	nc	nc	nc
2^{-8}	57.2	12.6	10.2	11.9	15.7	24.0	42.2	79.9	66.9	48.4	29.0
2^{-6}	127	12.0	4.69	5.56	7.16	10.4	13.2	15.5	17.4	16.2	12.9
2^{-4}	84.4	16.2	6.63	3.41	3.29	4.57	5.74	7.13	7.76	7.71	5.94
2^{-2}	118	23.0	9.27	4.27	2.05	1.84	2.41	3.04	3.75	3.66	2.60
2^{0}	175	24.5	10.9	5.11	2.11	1.15	1.02	1.49	1.87	1.82	1.38
2^{2}	146	24.5	11.5	5.07	2.25	1.15	0.68	0.77	1.00	0.96	0.87
2^{4}	118	21.7	10.2	4.77	2.33	1.28	0.74	0.59	0.61	0.59	0.57
2^{6}	109	20.0	9.46	4.79	2.58	1.41	0.78	0.60	0.58	0.58	0.56
2^{8}	145	18.7	9.38	4.73	2.54	1.49	0.92	0.58	0.57	0.55	0.53
2^{10}	187	19.3	9.25	4.60	2.22	1.32	0.81	0.55	0.55	0.52	0.47

(b) FLOP counts (billions)

Table 1: Computational results with FCDSA for a realistic hetereogeneous problem containing two materials whose total cross sections are $\sigma_{t,1}$ and $\sigma_{t,2}$ (cm^{-1}). An entry "nc" indicates that the problem did not converge in 4 CPU hours.

$\sigma_{t,1}$	$\sigma_{t,2}$										
	2^{-10}	2^{-8}	2−6	2^{-4}	2^{-2}	2^{0}	2^{2}	2^{4}	2^{6}	2^{8}	2^{10}
2^{-10}	4	4	6	8	13	34	109	242	345	344	205
2^{-8}	5	5	6	8	13	33	103	222	316	317	190
2^{-6}	6	6	6	8	13	30	86	174	254	259	164
2^{-4}	9	9	9	9	12	24	60	117	173	184	127
2^{-2}	14	14	14	13	11	18	40	77	114	125	97
2^{0}	32	31	30	25	18	21	40	72	103	115	96
2^{2}	89	87	80	64	44	41	60	87	128	143	124
2^{4}	182	177	160	126	84	73	98	123	163	184	177
2^{6}	244	235	211	164	109	90	123	150	182	206	208
2^{8}	272	261	229	176	118	91	119	147	188	208	204
2^{10}	186	178	160	131	88	72	94	132	185	198	160

(a) Number of iterations

$\sigma_{t,1}$	$\sigma_{t,2}$										
	2^{-10}	2^{-8}	2^{-6}	2^{-4}	2^{-2}	2^{0}	2^{2}	2^{4}	2^{6}	2^{8}	2^{10}
2^{-10}	0.10	0.10	0.14	0.17	0.27	0.69	2.18	4.82	6.87	6.84	4.08
2^{-8}	0.12	0.12	0.14	0.17	0.27	0.67	2.06	4.42	6.29	6.30	3.78
2^{-6}	0.14	0.14	0.14	0.17	0.27	0.61	1.72	3.46	5.05	5.15	3.26
2^{-4}	0.20	0.20	0.19	0.19	0.25	0.49	1.20	2.33	3.44	3.66	2.52
2^{-2}	0.30	0.30	0.30	0.27	0.23	0.37	0.81	1.54	2.27	2.48	1.93
2^{0}	0.66	0.64	0.62	0.51	0.37	0.43	0.8	1.44	2.05	2.28	1.90
2^{2}	1.80	1.76	1.61	1.29	0.89	0.82	1.20	1.73	2.54	2.82	2.44
2^{4}	3.67	3.56	3.21	2.53	1.68	1.45	1.95	2.44	3.21	3.62	3.47
2^{6}	4.91	4.72	4.23	3.28	2.17	1.79	2.44	2.96	3.57	4.03	4.07
2^{8}	5.48	5.25	4.59	3.52	2.35	1.81	2.35	2.90	3.68	4.06	3.98
2^{10}	3.75	3.58	3.21	2.62	1.75	1.43	1.86	2.60	3.62	3.86	3.12

(b) FLOP counts (billions)

Table 2: Computational results with the S–WLA scheme for a realistic hetereogeneous problem containing two materials whose total cross sections are $\sigma_{t,1}$ and $\sigma_{t,2}$ (cm^{-1}). An entry "nc" indicates that the problem did not converge in 4 CPU hours.

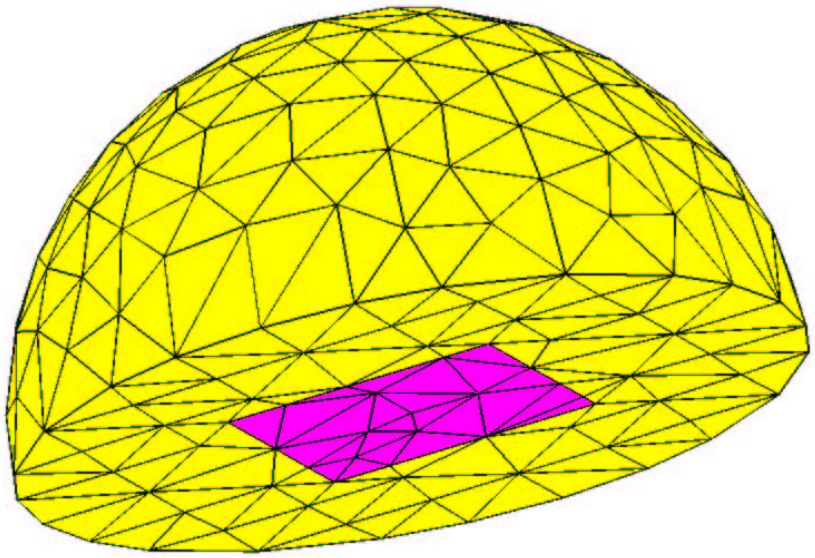

Figure 13: Mesh for a realistic heterogeneous problem consisting of two different materials as indicated by the shading in the figure. The bottom face is reflective and the box contains a unit isotropic distributed source.

that if the method is to be practical then the spectral radius must be small enough to warrant the expense of solving these linear systems at every transport iteration. The degradation in the spectral radius seen here implies that we cannot expect the method to be efficient in general. This is especially true for heterogeneous problems that contain optically thick, diffusive, regions together with optically thin, streaming–dominated regions, such as problems with ducts surrounded by highly scattering materials. Furthermore, the partially consistent S–WLA method also loses its effectiveness and is even more affected by the material discontinuities in such heterogeneous problems. Efficient transport solutions may not be attainable even though the linear systems associated with the S–WLA method can be solved relatively easily.

So we are left with a situation where there is no DSA method which is clearly unconditionally effective and efficient. However, in Part II of this paper we will present an approach that restores effectiveness of the S–WLA method over a wide range of problems. We will show that the relatively inexpensive computations involved in this DSA scheme enable us to once again efficiently compute transport solutions in the kinds of optically thick, heterogeneous problems examined here.

Acknowledgments

This work was performed under the auspices of the U.S. Department of Energy at the Los Alamos National Laboratory. The authors would like to thanks Marvin Adams of Texas A&M University for his helpful discussions.

A Asymptotic–Preserving Lumping on Tetrahedra

In this appendix we derive a lumped linear-discontinuous finite-element tetrahedral-mesh discretization for the S_N equations that has excellent properties in the thick diffusion limit. The variational formulation for the linear discontinuous discretization is given in Section 2.1. The discretization has one angular flux unknown at each vertex i, denoted by ψ_i. We can illustrate the discretizations and their asymptotic properties by considering just a single vertex. The vertex indexing for a tetrahedron is illustrated in Fig. 14. Angular indices and cell indices will be suppressed for simplicity.

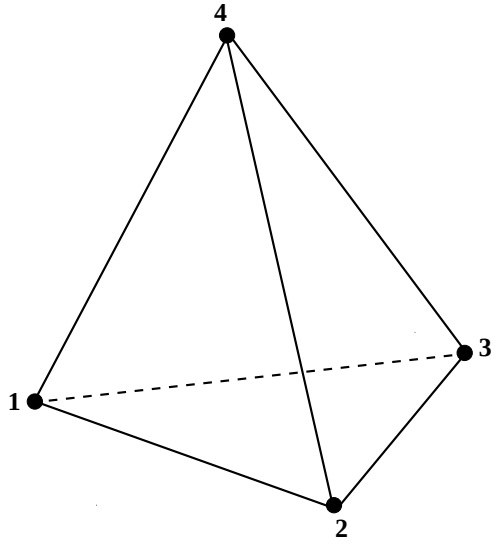

Figure 14: Tetrahedron vertex indexing.

Our first task is to describe the unlumped equations in detail. Using linear basis and trial functions in Eqs. 3, the unlumped equation for vertex $j = 1$ is

$$\begin{aligned}\frac{1}{4}\left[\psi_1+\psi_2+\psi_3+\psi_4\right]\left(\frac{1}{3}\hat{\Omega}\cdot\overrightarrow{A_1}\right)+\frac{1}{4}\left[2\psi_1^b+\psi_3^b+\psi_4^b\right]\left(\frac{1}{3}\hat{\Omega}\cdot\overrightarrow{A_2}\right)\\ \frac{1}{4}\left[2\psi_1^b+\psi_2^b+\psi_4^b\right]\left(\frac{1}{3}\hat{\Omega}\cdot\overrightarrow{A_3}\right)+\frac{1}{4}\left[2\psi_1^b+\psi_2^b+\psi_3^b\right]\left(\frac{1}{3}\hat{\Omega}\cdot\overrightarrow{A_4}\right)\\ +\sigma_t\frac{1}{5}\left[2\psi_1+\psi_2+\psi_3+\psi_4\right]\frac{V}{4}=\frac{1}{5}\left[2q_1+q_2+q_3+q_4\right]\frac{V}{4},\end{aligned} \tag{8}$$

where we have suppressed the cell index k and angular index m. In this expression ψ_j^b denotes a boundary flux defined in Eq. (3b), $\hat{\Omega}$ is a unit direction vector, $\overrightarrow{A_i}$ is the outwardly directed area vector for face i, V denotes the volume of the tetrahedron, and q_i denotes the total source for vertex i, which is the sum of the scattering and inhomogeneous sources, or

$$q_i = \sigma_s\phi_i + Q_i \ . \tag{9}$$

We assume isotropic scattering and isotropic inhomogeneous sources. The area vector is the integral of the outwardly directed normal unit vector over a face, that is,

$$\overrightarrow{A} = \int_A \hat{n}\, dA\,. \tag{10}$$

The lumping process is well defined for the surface leakage, removal and source terms in Eq. (8). In particular, one simply replaces the weighted volumetric averages for these terms with ψ_1 and q_1 respectively, for example,

$$\frac{1}{4}\Big[2\psi_1^b + \psi_3^b + \psi_4^b\Big] \quad \longrightarrow \quad \psi_1, \tag{11}$$

$$\frac{1}{4}\Big[2\psi_1^b + \psi_2^b + \psi_4^b\Big] \quad \longrightarrow \quad \psi_1, \tag{12}$$

$$\frac{1}{4}\Big[2\psi_1^b + \psi_2^b + \psi_3^b\Big] \quad \longrightarrow \quad \psi_1, \tag{13}$$

$$\frac{1}{5}\Big[2\psi_1 + \psi_2 + \psi_3 + \psi_4\Big] \quad \longrightarrow \quad \psi_1, \tag{14}$$

$$\frac{1}{5}\Big[2q_1 + q_2 + q_3 + q_4\Big] \quad \longrightarrow \quad q_1. \tag{15}$$

Following the prescription given in Eqs. (11) through (15), the surface-lumped, removal-lumped and source-lumped version of Eq. (8) is

$$\frac{1}{4}\Big[\psi_1 + \psi_2 + \psi_3 + \psi_4\Big]\left(\frac{1}{3}\hat{\Omega}\cdot\overrightarrow{A_1}\right) + \psi_1^b\left(\frac{1}{3}\hat{\Omega}\cdot\overrightarrow{A_2}\right) + \psi_1^b\left(\frac{1}{3}\hat{\Omega}\cdot\overrightarrow{A_3}\right) + \psi_1^b\left(\frac{1}{3}\hat{\Omega}\cdot\overrightarrow{A_4}\right) + \sigma_t\psi_1\frac{V}{4} = \sigma_t q_1\frac{V}{4}\,. \tag{16}$$

We now consider the behavior of the discretization represented by Eq. (16) in the thick diffusion limit through an asymptotic analysis.[15–17] First, we scale the problem as follows:

$$\sigma_t \quad \longrightarrow \quad \sigma_t/\epsilon\,, \tag{17}$$

$$\sigma_a \quad \longrightarrow \quad \sigma_a\epsilon\,, \tag{18}$$

$$\sigma_s \quad \longrightarrow \quad \sigma_t/\epsilon - \sigma_a\epsilon\,, \tag{19}$$

$$q \quad \longrightarrow \quad q\epsilon\,, \tag{20}$$

where ϵ is a small parameter. Next, the angular flux is expanded in powers of ϵ

$$\psi = \sum_{n=0}^{\infty}\psi^{(n)}\epsilon^n\,, \tag{21}$$

where $\psi^{(n)}$ denotes the asymptotic components of the solution multiplied by ϵ^n. Finally, Eq. (21) is substituted into the scaled transport equation and the coefficients for each power of ϵ are equated to obtain a

heirarchy of equations ordered by index n. When this procedure is applied to the analytic transport equation, the leading–order scalar flux satisfies the diffusion equation

$$-\overrightarrow{\nabla}\cdot\frac{1}{3\sigma_t}\overrightarrow{\nabla}\phi^{(0)}+\sigma_a\phi^{(0)}=q\ , \tag{22}$$

the leading-order currents are identically zero,

$$\overrightarrow{J}^{(0)}=\overrightarrow{0}\ , \tag{23}$$

and the first-order currents satisfy Fick's law,

$$\overrightarrow{J}^{(1)}=-\frac{1}{3}\overrightarrow{\nabla}\phi^{(0)}\ . \tag{24}$$

When applied to S_N discretization scheme represented by Eq. (16), the asymptotic scaling yields an accurate discretization of the diffusion equation for the leading–order scalar flux on the mesh interior that is identical to the lumped linear–continuous finite-element discretization. However, while this scheme yields correct leading-order currents that are identically zero, it also yields first-order currents that are incorrect in that they are not exact for a linearly-dependent scalar flux. For example, at vertex 1 the expression for the first-order current is

$$\overrightarrow{J}_1^{(1)}=-\frac{1}{3\sigma_t}\left\{\frac{1}{V}\left[\frac{1}{3}\left(\phi_2^{(0)}+\phi_3^{(0)}+\phi_4^{(0)}\right)-\phi_1^{(0)}\right]\overrightarrow{A_1}\right\}\ . \tag{25}$$

This expression is clearly wrong for an arbitrary linear dependence of $\phi^{(0)}$ because the current is always directed along $\overrightarrow{A_1}$. Such a situation is highly undesirable because the currents calculated in a highly diffusive problem are dominated by the first-order currents. It is difficult to imagine how the correct scalar fluxes are obtained when the currents are incorrect. However, some insight can be gained without going into too much detail. Begin by noting that the average of the four vertex current expressions is in fact exact for an arbitrary linear dependence of $\phi^{(0)}$. Again consider the expressions for vertex 1:

$$\overrightarrow{J}_{avg}^{(1)}=-\frac{1}{3\sigma_t}\left\{-\frac{1}{3V}\left(\phi_1^{(0)}\overrightarrow{A_1}+\phi_2^{(0)}\overrightarrow{A_2}+\phi_3^{(0)}\overrightarrow{A_3}+\phi_4^{(0)}\overrightarrow{A_4}\right)\right\}. \tag{26}$$

The accuracy of this expression can be recognized through the integral identity

$$\left(\overrightarrow{\nabla}\phi^{(0)}\right)_{avg}=\frac{1}{V}\int_V\overrightarrow{\nabla}\phi^{(0)}\,dV=\oint_{\delta V}\phi^{(0)}\hat{n}\,dA\ . \tag{27}$$

If $\phi^{(0)}$ has a linear dependence then its gradient will be constant. Thus the gradient at each vertex will be equal to the average gradient. The expression inside the curly brackets in Eq. (26) follows directly from a

straightforward discretization of the surface integral in Eq. (27) that is exact for a linear dependence of $\phi^{(0)}$. This is most easily seen by re–expressing Eq. (26) as follows:

$$\begin{aligned}\overrightarrow{J}_{avg}^{(1)} = -\frac{1}{3\sigma_t}\Bigg\{\frac{1}{V}\Bigg[\frac{1}{3}\left(\phi_2^{(0)}+\phi_3^{(0)}+\phi_4^{(0)}\right)\overrightarrow{A_1}+\frac{1}{3}\left(\phi_1^{(0)}+\phi_3^{(0)}+\phi_4^{(0)}\right)\overrightarrow{A_2} \\ +\frac{1}{3}\left(\phi_1^{(0)}+\phi_2^{(0)}+\phi_4^{(0)}\right)\overrightarrow{A_3}+\frac{1}{3}\left(\phi_1^{(0)}+\phi_2^{(0)}+\phi_3^{(0)}\right)\overrightarrow{A_4}\Bigg]\Bigg\}\,,\end{aligned} \tag{28}$$

Equation (28) reduces to Eq. (26) taking into account that the area vectors sum to zero.

The inaccuracy of the first-order currents is eliminated by manipulating and and then lumping the interior leakage term in Eq. (16). For instance, we can first rewrite Eq. (16) as

$$\begin{aligned}-\frac{1}{4}\Big[\psi_1+\psi_2+\psi_3+\psi_4\Big]\left(\frac{1}{3}\hat{\Omega}\cdot\overrightarrow{A_2}\right)-\frac{1}{4}\Big[\psi_1+\psi_2+\psi_3+\psi_4\Big]\left(\frac{1}{3}\hat{\Omega}\cdot\overrightarrow{A_3}\right)-\frac{1}{4}\Big[\psi_1+\psi_2+\psi_3+\psi_4\Big]\left(\frac{1}{3}\hat{\Omega}\cdot\overrightarrow{A_4}\right) \\ +\psi_1^b\left(\frac{1}{3}\hat{\Omega}\cdot\overrightarrow{A_2}\right)+\psi_1^b\left(\frac{1}{3}\hat{\Omega}\cdot\overrightarrow{A_3}\right)+\psi_1^b\frac{1}{3}\left(\frac{1}{3}\hat{\Omega}\cdot\overrightarrow{A_4}\right)+\sigma_t\psi_1\frac{V}{4}=\sigma_t q_1\frac{V}{4}\,,\end{aligned} \tag{29}$$

and then lump the internal leakage terms:

$$\frac{1}{4}\Big[\psi_1+\psi_2+\psi_3+\psi_4\Big]\left(\frac{1}{3}\hat{\Omega}\cdot\overrightarrow{A_i}\right) \quad\rightarrow\quad \frac{1}{4}\Big[\psi_1+3\psi_i\Big]\left(\frac{1}{3}\hat{\Omega}\cdot\overrightarrow{A_i}\right), \quad \text{for} \quad i=2,3,4. \tag{30}$$

This yields the following fully lumped S_N discretization scheme:

$$\begin{aligned}-\frac{1}{4}\Big[\psi_1+3\psi_2\Big]\left(\frac{1}{3}\hat{\Omega}\cdot\overrightarrow{A_2}\right)-\frac{1}{4}\Big[\psi_1+3\psi_3\Big]\left(\frac{1}{3}\hat{\Omega}\cdot\overrightarrow{A_3}\right)-\frac{1}{4}\Big[\psi_1+3\psi_4\Big]\left(\frac{1}{3}\hat{\Omega}\cdot\overrightarrow{A_4}\right) \\ +\psi_1^b\left(\frac{1}{3}\hat{\Omega}\cdot\overrightarrow{A_2}\right)+\psi_1^b\left(\frac{1}{3}\hat{\Omega}\cdot\overrightarrow{A_3}\right)+\psi_1^b\left(\frac{1}{3}\hat{\Omega}\cdot\overrightarrow{A_4}\right)+\sigma_t\psi_1\frac{V}{4}=\sigma_t q_1\frac{V}{4}\,.\end{aligned} \tag{31}$$

Applying the asymptotic analysis to this discretization gives an expression for the first–order current at vertex 1 that is exact for any linearly–dependent $\phi^{(0)}$. That is,

$$\overrightarrow{J}_1^{(1)} = -\frac{1}{3\sigma_t}\Bigg\{-\frac{1}{3V}\left(\phi_1^{(0)}\overrightarrow{A_1}+\phi_2^{(0)}\overrightarrow{A_2}+\phi_3^{(0)}\overrightarrow{A_3}+\phi_4^{(0)}\overrightarrow{A_4}\right)\Bigg\}\,, \tag{32}$$

which is identical to $\overrightarrow{J}_{avg}^{(1)}$ given in Eq. (26). Furthermore, this same expression is obtained for every vertex which is to be expected because the linear finite element approximation implies a constant gradient within the tetrahedron. We emphasize that the S_N discretization defined by Eq. (31) calculates accurate currents in highly diffusive problems while the scheme defined by Eq. (16) does not, even though they both yield the same leading–order interior-mesh asymptotic diffusion discretization.

References

1. R. E. Alcouffe, "Diffusion Synthetic Acceleration Methods for Diamond-Differenced Discrete-Ordinates Equations," *Nucl. Sci. Engr.*, **64**, pp. 344–355 (1977).

2. E. W. Larsen, "Unconditionally Stable Diffusion-Synthetic Acceleration Methods for Slab Geometry Discrete Ordinates Equations. Part I: Theory," *Nucl. Sci. Engr.*, **82**, pp. 47–63 (1982).

3. D. R. McCoy and E. W. Larsen, "Unconditionally Stable Diffusion-Synthetic Acceleration Methods for Slab Geometry Discrete Ordinates Equations. Part II: Numerical Results," *Nucl. Sci. Engr.*, **82**, pp. 64–70 (1982).

4. M. L. Adams and T. A. Wareing, "Diffusion-Synthetic Acceleration Given Anisotropic Scattering, General Quadratures, and Multidimensions," *Trans. of the Am. Nucl. Soc.*, **68**, pp. 203–204 (1993).

5. J. S. Warsa, T. A. Wareing, and J. E. Morel, "Fully Consistent Diffusion Synthetic Acceleration of Linear Discontinuous Transport Discretizations on Three-Dimensional Unstructured Meshes," *Nucl. Sci. Engr.*, **141**, pp. 236–251 (2002).

6. T. A. Wareing, "New Diffusion-Synthetic Accelerations Methods for the S_N Equations with Corner Balance Spatial Differencing," in **Joint International Conference on Mathematical Methods and Supercomputing in Nuclear Applications**, 19-23 April, Vol. 2, Karlsruhe, Germany, p. 500 (1993).

7. T. A. Wareing, J. M. McGhee, and J. E. Morel, "ATTILA: A Three-Dimensional, Unstructured Tetrahedral Mesh Discrete Ordinates Transport Code," *Transactions of the American Nuclear Society*, **75**, pp. 146–147 (1996).

8. M. L. Adams and W. R. Martin, "Diffusion Synthetic Acceleration of Discontinuous Finite Element Transport Iterations," *Nucl. Sci. Engr.*, **111**, pp. 145–167 (1992).

9. Y. Azmy, "Impossibility of Unconditional Stability and Robustness of Diffusive Accleration Schemes," in **1998 American Nuclear Society Radiation Protection and Shielding Division Topical Meeting**, 19-23 Apr, Vol. 1, Nashville, TN, p. 480 (1998).

10. T. A. Wareing, J. M. McGhee, J. E. Morel, and S. D. Pautz, "Discontinuous Finite Element S_n Methods on Three-Dimensional Unstructured Grids," *Nucl. Sci. Engr.*, **138**, pp. 256–268 (2001).

11. E. E. Lewis and W. F. Miller, **Computational Methods of Neutron Transport**. Wiley & Sons: New York (1984).

12. H. J. Kopp, "Synthetic Method Solution of the Transport Equation," *Nucl. Sci. Engr.*, **17**, p. 65 (1963).

13. E. M. Gelbard and L. A. Hageman, "The Synthetic Method as Applied to the S_n Equations," *Nucl. Sci. Engr.*, **37**, pp. 288–298 (1969).

14. R. E. Alcouffe, "Diffusion Synthetic Acceleration Methods for the Diamond-Differenced Discrete-Ordinate Equations," *Nucl. Sci. Engr.*, **64**, pp. 344–355 (1977).

15. E. W. Larsen, J. E. Morel, and W. F. Miller, Jr., "Asymptotic Solutions of Numerical Transport Problems in Optically Thick, Diffusive Regimes I," *J. Comp. Phys.*, **69**, pp. 283–324 (1987).

16. E. W. Larsen and J. E. Morel, "Asymptotic Solutions of Numerical Transport Problems in Optically Thick, Diffusive Regimes II," *J. Comp. Phys.*, **83**, pp. 212–236 (1989).

17. M. L. Adams, "Discontinuous Finite Element Methods in Thick Diffusive Problems," *Nucl. Sci. Engr.*, **137**, pp. 298–333 (2001).